

# Mixed Ionic Liquids: The Case of Pyridinium-Based Fluids

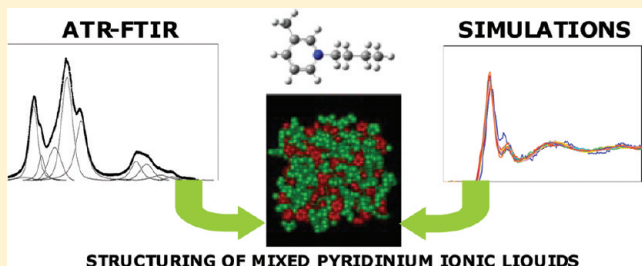
Santiago Aparicio\*,† and Mert Atilhan‡

†Department of Chemistry, University of Burgos, 09001 Burgos, Spain

‡Chemical Engineering Department, Qatar University, Doha, Qatar

## Supporting Information

**ABSTRACT:** We report in this work a combined experimental and computational study on the molecular level structuring of binary ionic liquid mixtures comprising pyridinium cations. The effect of anions on liquid structure was analyzed from the mixing (mixture 1) of  $[b3mpy][BF_4]$  and  $[b3mpy][N(CN)_2]$  ionic liquids, in the full composition range, leading to  $[b3mpy][BF_4]_x[N(CN)_2]_{1-x}$  mixed ionic liquids. The effect of the length of alkylic chains in cations was studied with mixtures (mixture 2) of  $[b3mpy][BF_4]$  and  $[o3mpy][BF_4]$  ionic liquids, also studied in the full composition range, leading to  $[b3mpy]_x[o3mpy]_{1-x}[BF_4]$  ionic liquids. Fourier transform infrared–attenuated total reflection spectra were recorded and analyzed as a function of anionic and cationic composition for the two studied mixture types. Classical molecular dynamics simulations were also performed for mixtures 1 and 2 as a function of anionic and cationic composition. The reported experimental and computational results show that the properties of the studied mixed systems change in an almost linear way, leading to almost ideal mixtures from the thermodynamic viewpoint, and thus pointing to simple dilution effects of the involved ions controlling the mixture properties.



STRUCTURING OF MIXED PYRIDINIUM IONIC LIQUIDS

## 1. INTRODUCTION

Ionic liquids have attracted a great interest both in the industry and academia in the last years.<sup>1–4</sup> The main reason of this interest is the possibility of designing fluids with the most adequate characteristics required for each chemical or industrial process through a judicious combination of anions and cations.<sup>5–7</sup> Therefore, ionic liquids may be considered as tailor-made fluids<sup>8,9</sup> considering the enormous amount of possible anion–cation combinations leading to ionic liquids.<sup>10</sup> Most of the studies available in the open literature have considered the properties and behavior of pure ionic liquids or of ionic liquids mixed with common organic solvents, and a reduced number of works have analyzed the properties of mixed ionic liquids.<sup>11–16</sup> Nevertheless, the new chemistry rising from ionic liquids may be extended even further through the mixing of ionic liquids, that is to say, having ionic liquids with several types of anions and/or cations. Studies on mixed ionic liquids are almost absent in the literature in our opinion because of the large number of pure ionic liquids that are under study and the poor knowledge in most of the cases of the relationships between their properties and molecular structure, which hinders the studies on the more complex ionic liquid multicomponent mixtures.

The study of binary mixtures of ionic liquids should be the first step to extend the knowledge from pure ionic liquids to complex mixtures involving several anions and/or cations. A binary ionic liquid mixture comprising a common cation  $A^+$  and two different anions  $X^-$  and  $Y^-$  (obtained from the mixing of two ionic liquids  $AX$  and  $AY$  at different ratios) is strictly speaking a ternary system, but it is also a complex ionic liquid

containing one cation and two anions,  $AX_xY_y$ , with  $x$  and  $y$  ratios tuned through the amounts of mixed  $AX$  and  $AY$  ionic liquids. Analogous considerations may be done for binary mixtures comprising one common anion and two different cations. The presence of two types of ions of the same charge competing for the interaction with ions of opposite charge, and developing interactions between them, should lead to new effects and properties not present in ionic liquids composed by one type of anions and cations. From a thermodynamic viewpoint, Canongia et al.<sup>12</sup> analyzed the deviations from ideality in binary mixtures of ionic liquids containing a common ion, centering their analysis on imidazolium-based fluids. Results by Canongia et al.<sup>12</sup> showed a quasi-ideal behavior for the studied mixtures, with increasing nonidealities as the size differences between the involved cations increases. Analogous results were obtained by Navia et al.<sup>15</sup> and Stoppa et al.<sup>16</sup> This quasi ideal behavior for the studied binary mixtures of ionic liquids is highly surprising considering the complexity of the intermolecular forces appearing in these mixed fluids. Moreover, most of the scarce available studies are centered on imidazolium-based ionic liquids, and thus, studies on mixtures involving other families of ions are required. Therefore, further systematic studies analyzing molecular-level behavior of binary mixtures of ionic liquids are highly recommended to infer the subtle structural and energetic features rising from the mixing process.

Received: December 20, 2011

Revised: February 6, 2012

Published: February 6, 2012

In previous works, we analyzed the properties of pyridinium-based ionic liquids using a combined experimental and computational approach to shed light into the molecular level features controlling fluids structuring and relevant industrial properties such as viscosity.<sup>17</sup> We have analyzed the effects of anion types and alkylic chains length and positions in the pyridinium cations. Therefore, we extend these studies in this work to the analysis of binary mixtures of pyridinium-based ionic liquids to advance in the knowledge of mixed fluids based on ionic liquids. We have selected two types of mixtures in this work: (i) binary mixtures of  $[b3mpy][BF_4]$  (1-butyl-3-methylpyridinium tetrafluoroborate) and  $[b3mpy][N(CN)_2]$  (1-butyl-3-methylpyridinium dicyanamide) ionic liquids (namely, mixture 1), leading to  $[b3mpy][BF_4]_x[N(CN)_2]_{1-x}$  (with  $x$  varying in the 0 to 1 mol fraction range) complex ionic liquids; (ii) binary mixtures of  $[b3mpy][BF_4]$  and  $[o3mpy][BF_4]$  (1-octyl-3-methylpyridinium tetrafluoroborate) ionic liquids (namely, mixture 2), leading to  $[b3mpy]_x[o3mpy]_{1-x}[BF_4]$  ionic liquid (with  $x$  varying in the 0 to 1 mol fraction range), Figure 1. The anionic and cationic

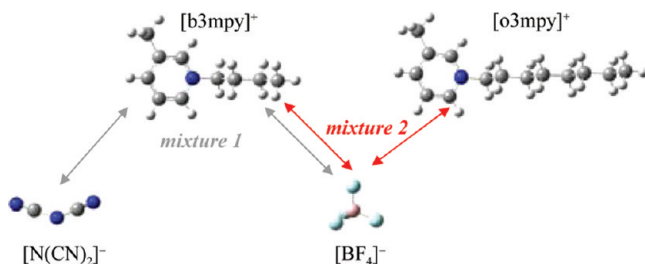


**Figure 1.** Molecular scheme of the ionic liquid binary mixtures studied in this work. Mixture 1 stands for  $[b3mpy][BF_4]_x[N(CN)_2]_{1-x}$  and  $[b3mpy]_x[o3mpy]_{1-x}[BF_4]$ , with  $x$  varying in the 0 to 1 mol fraction range) and mixture 2 for  $[b3mpy][BF_4] + [o3mpy][BF_4]$  ( $[b3mpy]_x[o3mpy]_{1-x}[BF_4]$ , with  $x$  varying in the 0 to 1 mol fraction range). Atomic color code: gray, carbon; light gray, hydrogen; blue, nitrogen; pink, boron; and light blue, fluorine.

ratio in  $[b3mpy][BF_4]_x[N(CN)_2]_{1-x}$  and  $[b3mpy]_x[o3mpy]_{1-x}[BF_4]$  was controlled through the amounts of pure ionic liquids used in the preparation of mixtures, which were studied in the full range. The properties of these mixtures were analyzed using a double approach: (i) infrared spectroscopy and (ii) molecular dynamics simulations. This combined experimental-computational approach has been used by our group in previous works to shed light into the molecular-level structure of complex systems involving ionic liquids.<sup>18,19</sup>

## 2. MATERIALS AND METHODS

**2.1. Materials.**  $[b3mpy][BF_4]$  (CAS no: 597581-48-1, 99% purity),  $[b3mpy][N(CN)_2]$  (CAS no: 712355-12-9, 98% purity), and  $[o3mpy][BF_4]$  (CAS no: 712355-10-7, 98% purity) ionic liquid samples were provided by Solvent Innovation. Samples were dried under vacuum with stirring at 333 K for 24 h, then stored in Schlenk flasks. The water content was measured before any measurement through Karl Fischer coulometric titration ( $\pm 0.3\%$  in water mass content), and it was 450, 300, and 230 ppm for  $[b3mpy][BF_4]$ ,  $[b3mpy][N(CN)_2]$ , and  $[o3mpy][BF_4]$ , respectively.  $^1H$  and  $^{19}F$  NMR did not show any remarkable impurity, and thus, no further additional purification procedures were considered. Samples were handled under nitrogen atmosphere in glove boxes. Mixtures were

prepared in the full composition range by weighing with a Mettler AT261 balance ( $\pm 1 \times 10^{-5}$  g), thus leading to  $\pm 1 \times 10^{-4}$  for mole fraction.

**2.2. Experimental Measurements.** Attenuated total reflection infrared (ATR-FTIR) spectroscopy studies were developed with a Nicolet Nexus spectrometer together with a Smart Thermal ARK device. The ATR accessory contains a zinc selenide crystal, the temperature of which is controlled through a built-in controller, and measured through an RTD temperature sensor to  $\pm 1$  °C. Refractive indexes for the sodium D-line were measured to  $\pm 1 \times 10^{-5}$  with an automated Leica AR600 refractometer whose temperature was controlled by a Julabo F32 external circulator and measured with a built-in thermometer to  $\pm 1 \times 10^{-2}$  K. Refractometer calibration was done using water and a standard supplied by the manufacturer ( $n_D = 1.51416$ ).

**2.3. Molecular Modeling Methods.** Classical molecular dynamics simulations were carried out using the TINKER molecular modeling package.<sup>20</sup> All simulations were performed in the NPT ensemble; the Nosé-Hoover method<sup>21</sup> was used to control the temperature and pressure of the simulation systems. The motion equations were solved using the Verlet Leapfrog integration algorithm.<sup>22</sup> Long-range electrostatic interactions were treated with the smooth particle mesh Ewald method.<sup>23</sup> The simulated systems consist of cubic boxes, containing a variable number of anions and cations to analyze the whole composition range, Table 1. Periodic boundary conditions were

**Table 1. Systems Used for Molecular Dynamics Simulations of  $x [b3mpy][BF_4] + (1 - x) [b3mpy][N(CN)_2]$  and  $x [b3mpy][BF_4] + (1 - x) [o3mpy][BF_4]$  Binary Mixtures<sup>a</sup>**

$x$	$N ([b3mpy][BF_4])$	$N ([b3mpy][N(CN)_2])$ or $N ([o3mpy][BF_4])$
0	0	125
0.05	6	119
0.15	19	106
0.25	31	94
0.35	44	81
0.45	56	69
0.55	69	56
0.65	81	44
0.75	94	31
0.85	106	19
0.95	119	6
1	125	0

<sup>a</sup> $x$  stands for mole fraction. All simulations were performed at 298 K/0.1 MPa.

applied in the three directions to simulate an infinite system. The simulations were performed using a cutoff radius of 10 Å. Low density initial boxes ( $\sim 0.50$  g cm<sup>-3</sup>) were generated using the PACKMOL program<sup>24</sup> and were energetically minimized according to the MINIMIZE program in TINKER package to a 0.01 kcal mol<sup>-1</sup> Å<sup>-1</sup> rms gradient. Several heating and quenching steps in the NVT ensemble up to 500 K were performed after which a 100 ps NVT equilibration molecular dynamics simulation was run at 298 K. Finally, from the output NVT simulation configuration, a run of 10 ns (time step 1 fs) in the NPT ensemble at 298 K/0.1 MPa was run, from which the first 5 ns were used to ensure equilibration (checked through constant energy) and the remaining 5 ns for data collection. Several uncorrelated initial boxes were built for each mixed ionic liquid, no remarkable differences were found between

properties obtained from the simulations using different initial conditions. The used force field parametrization for the studied pyridinium based ionic liquids was reported and validated in a previous work.<sup>17</sup>

### 3. RESULTS AND DISCUSSION

**3.1. ATR-FTIR Spectroscopy Results.** [b3mpy][BF<sub>4</sub>]<sub>x</sub>[N-(CN)<sub>2</sub>]<sub>1-x</sub> and [b3mpy]<sub>x</sub>[o3mpy]<sub>1-x</sub>[BF<sub>4</sub>] mixtures were studied in the 400–4000 cm<sup>-1</sup> spectral range, although we will center our analysis in the 2800–3200 cm<sup>-1</sup> range, which leads to the most relevant conclusions. Results for the three studied pure pyridinium-based ionic liquids are reported in Figure 2, together with the Gaussian–Lorentzian deconvolution

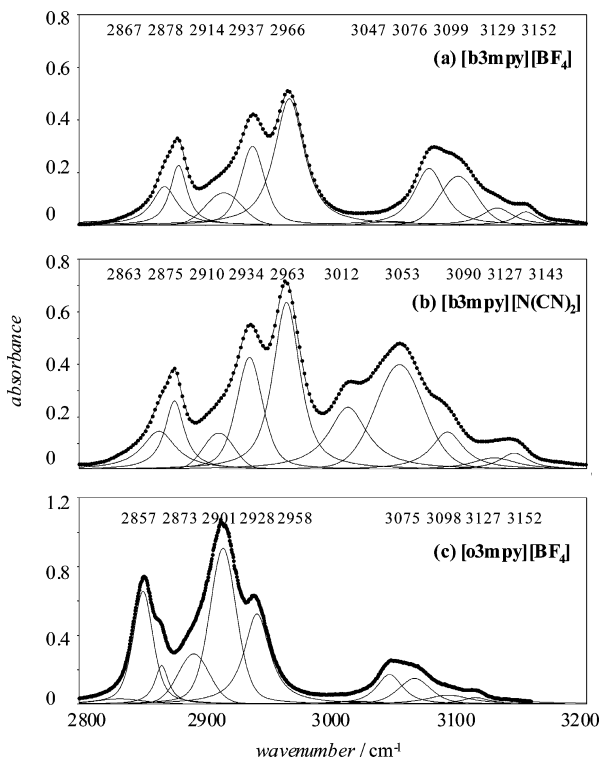


**Figure 2.** Deconvolution of the ATR-FTIR spectra in the 2800–3200 cm<sup>-1</sup> range, for pure pyridinium-based ionic liquids ionic liquids at 298 K. Symbols: ●, experimental data; lines, deconvoluted spectra. Spectra were deconvoluted using Gaussian–Lorentzian functions. Numeric values within each panel show the position of the corresponding deconvoluted peaks in cm<sup>-1</sup>.

tion peaks (Tables S1 and S2, Supporting Information). Spectra for [b3mpy][BF<sub>4</sub>]<sub>x</sub>[N(CN)<sub>2</sub>]<sub>1-x</sub> binary mixture are reported in Figure 3 and the deconvoluted spectra in Table S1 (Supporting Information). Before doing further analysis of ATR-FTIR results, we should make some comments about the experimental procedures. It is well-known that for ATR measurements, absorbance is directly proportional to the path length (*d*), in such a way that effective path length (*d<sub>e</sub>*) at each reflection is twice the penetration depth of the evanescent wave in the ATR system, defined according to eq 1.<sup>25</sup>

$$d_e = \frac{2}{k} \left( n_1 \sqrt{\sin^2 \theta - (n_2/n_1)^2} \right)^{-1} \quad (1)$$

where *k* is the wave vector of the light for vacuum,  $\theta$  is the incident angle (=45° in our experiments), and *n*<sub>1</sub> (=2.4 in the

studied wavelength range) and *n*<sub>2</sub> are the refractive indexes of the prism and the sample, respectively, at the wavelengths for which ATR measurements are performed. Therefore, *d<sub>e</sub>*, and thus absorbance at each wavelength, depends on the refractive index of the sample at each wavelength. We have measured the refractive index of [b3mpy][BF<sub>4</sub>]<sub>x</sub>[N(CN)<sub>2</sub>]<sub>1-x</sub> and for [b3mpy]<sub>x</sub>[o3mpy]<sub>1-x</sub>[BF<sub>4</sub>] mixtures, for the sodium D-line (589.3 nm, *n*<sub>D</sub>), Figure 4, and an almost linear variation with mole fraction is obtained. To correct ATR spectra according to eq 1, we should have information on the changes of refractive indexes for all the studied mixtures and pure fluids, as a function of radiation wavelength. We do not have such experimental information, and thus, we have analyzed the possible changes of *d<sub>e</sub>* in an approximate way. Hasse et al.<sup>26</sup> analyzed the refractive indexes, *n*, of imidazolium-based ionic liquids as a function of radiation wavelength, and proposed eq 2 to correlate the variations with temperature and radiation wavelength.

$$n = n_0 + n_T T - \frac{\Delta n}{\Delta \lambda} (\lambda - \lambda_D) \quad (2)$$

where *T* stands for temperature,  $\lambda$  for the corresponding wavelength, and  $\lambda_D$  for the wavelength of the sodium D-line. Values reported by Hasse et al.<sup>26</sup> for  $\Delta n/\Delta \lambda$  for imidazolium-based ionic liquids are in the 450 to 630 cm<sup>-1</sup> range. We have considered that for the pyridinium-based ionic liquids studied in this work, and for their mixtures,  $\Delta n/\Delta \lambda$  should be in the same range (because *n*<sub>D</sub> values are also in the same range). Therefore, by neglecting the effect of *n*<sub>0</sub> and *n*<sub>T</sub> in eq 2, we have calculated *n* as function of radiation wavelength using the simplified eq 3, using  $\Delta n/\Delta \lambda$  values in the 400 to 600 cm<sup>-1</sup> range, and inferred the corresponding *d<sub>e</sub>* from eq 1.

$$n = n_D - \frac{\Delta n}{\Delta \lambda} (\lambda - \lambda_D) \quad (3)$$

Using this approach, the largest *d<sub>e</sub>* changes are obtained if  $\Delta n/\Delta \lambda = 400$  cm<sup>-1</sup>, both for [b3mpy][BF<sub>4</sub>] and [b3mpy][N-(CN)<sub>2</sub>] pure ionic liquids, in that case on going from pure [b3mpy][N(CN)<sub>2</sub>] to [b3mpy][BF<sub>4</sub>], *d<sub>e</sub>* would decrease around 11% in the 2800–3200 cm<sup>-1</sup> range (from 1.21 to 1.08 nm at 2800 cm<sup>-1</sup>, and from 1.09 to 0.97 nm at 3200 cm<sup>-1</sup>). For other possible combinations of  $\Delta n/\Delta \lambda$  values, lower variations of *d<sub>e</sub>* are obtained. Therefore, as the results reported in Figure 4 show linear variation of *n*<sub>D</sub> with mole fraction, we may expect that *d<sub>e</sub>* would decrease around 1% for each increasing 0.1 step in [b3mpy][BF<sub>4</sub>] mole fraction, and thus, absorbance should behave in the same way. Therefore, considering these low values of *d<sub>e</sub>* variations, and the absence of further *n* data, we have used the raw ATR data for the analysis of mixture properties. Analogous conclusions were inferred for [b3mpy]<sub>x</sub>[o3mpy]<sub>1-x</sub>[BF<sub>4</sub>] mixtures.

The comparison of the spectra for pure [b3mpy][N(CN)<sub>2</sub>] and [b3mpy][BF<sub>4</sub>], Figure 2a,b, shows that the main differences between both fluids appear in the 3000–3060 cm<sup>-1</sup> range. For wavelengths lower than 3000 cm<sup>-1</sup>, the spectra for both fluids are almost identical, and more subtle differences appear for the 3060–3200 cm<sup>-1</sup> range. For pure [b3mpy][N-(CN)<sub>2</sub>], Figure 2b, peaks at 2863, 2875, 2910, 2934, and 2963 cm<sup>-1</sup> (named peaks I to V, Table S1, Supporting Information) are assigned to symmetric stretching of CH<sub>2</sub>, symmetric stretching of CH<sub>3</sub>, antisymmetric stretching of CH<sub>2</sub>, Fermi resonance mode of CH<sub>3</sub>, and antisymmetric stretching of CH<sub>3</sub>, respectively, all for the groups in the butyl chain. These peaks

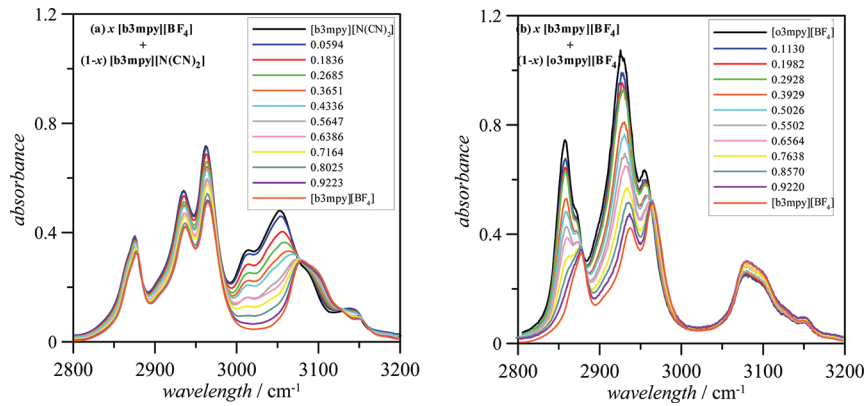


**Figure 3.** ATR-FTIR spectra of (a)  $x$  [b3mpy][BF<sub>4</sub>] + (1 -  $x$ ) [b3mpy][N(CN)<sub>2</sub>] and (b)  $x$  [b3mpy][BF<sub>4</sub>] + (1 -  $x$ ) [o3mpy][BF<sub>4</sub>] binary mixtures at 298 K. Values within each panel show [b3mpy]BF<sub>4</sub> mole fraction ( $x$ ).

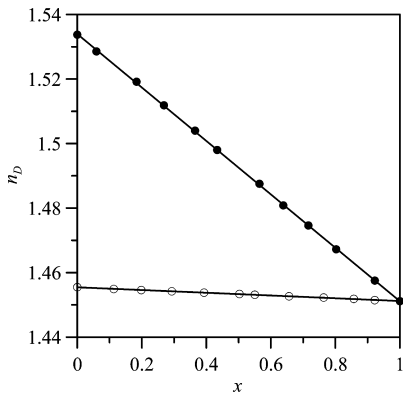


**Figure 4.** Refractive index for the sodium D-line in (●)  $x$  [b3mpy][BF<sub>4</sub>] + (1 -  $x$ ) [b3mpy][N(CN)<sub>2</sub>] and (○)  $x$  [b3mpy][BF<sub>4</sub>] + (1 -  $x$ ) [o3mpy][BF<sub>4</sub>] binary mixtures at 298 K.

appear at almost the same positions for butyl chains in [b3mpy][BF<sub>4</sub>], Figure 2a and Table S1 (Supporting Information); the only remarkable difference is the amplitude of the Fermi resonance mode of CH<sub>3</sub> (peak IV) and antisymmetric stretching of CH<sub>3</sub> (peak V), which decrease on going from [b3mpy][N(CN)<sub>2</sub>] to [b3mpy][BF<sub>4</sub>]. Moreover, peaks I to V, appear at almost the same positions as those corresponding to butyl chains in 1-butyl-3-methylimidazolium based ionic liquids (2856, 2877, 2913, 2938, and 2965 cm<sup>-1</sup> in 1-butyl-3-methylimidazolium tetrafluoroborate).<sup>27</sup> Therefore, bonding alkyl chains to pyridinium moieties does not change the vibrational properties of alkyl chains in comparison with common imidazolium-based compounds. Likewise, the type of anion does not change remarkably the peaks structuring in the region corresponding to alkylic chains.

Peak structuring in the 3000–3200 cm<sup>-1</sup> region is more complex, Figure 2a,b. For pure [b3mpy][N(CN)<sub>2</sub>], Figure 2b, five peaks may be inferred at 3012, 3053, 3090, 3127, and 3143 cm<sup>-1</sup> (named peaks VIa to X, Table S1, Supporting Information); the first two peaks (peak VIa and VII) were assigned to symmetric and antisymmetric stretching of the CH<sub>3</sub> group bonded to the pyridinium ring, respectively, and the last three peaks (peaks VIII to X) to stretching vibrations of CH groups in the pyridinium ring. These assignments are in agreement with the vibrational properties of 3-methylpyridine in this region.<sup>28</sup> Results for [b3mpy][BF<sub>4</sub>], Figure 2a, show five peaks (peaks VIb to X, Table S1, Supporting Information), which can be assigned to the same vibrational features as those

for [b3mpy][N(CN)<sub>2</sub>] (with the equivalence of peak VIa in [b3mpy][N(CN)<sub>2</sub>] with VIb in [b3mpy][BF<sub>4</sub>] all these peaks are blue-shifted in comparison with [b3mpy][N(CN)<sub>2</sub>]).

Results for the [b3mpy][BF<sub>4</sub>]<sub>x</sub>[N(CN)<sub>2</sub>]<sub>1-x</sub> mixture shows remarkable changes with increasing [b3mpy][BF<sub>4</sub>] mole fraction, Figure 3a. The results of peak deconvolution for this mixture are reported in Figure 5 for all the obtained peaks in the 2800–3200 cm<sup>-1</sup> range as a function of composition. In the region corresponding to butyl chain vibrations (peaks I to V), peaks do not suffer remarkable shifting, Figure 5 (I to V), and only peak intensity decreases on going from [b3mpy][N(CN)<sub>2</sub>] to [b3mpy][BF<sub>4</sub>], which could be justified considering a dilution effect because of the lower absorption of [b3mpy][BF<sub>4</sub>] in this region. The peak appearing at around 3012 cm<sup>-1</sup> (peak VIa) does not change its position, but its amplitude decreases linearly with increasing [b3mpy][N(CN)<sub>2</sub>] concentration, Figure 5 (VIa); therefore, this peak may be assigned exclusively to symmetric stretching vibrations of CH<sub>3</sub> groups bonded to pyridinium rings interacting with [N(CN)<sub>2</sub>] anions. For the 3040–3080 cm<sup>-1</sup> range, two well-defined regions are inferred, separated by 0.4–0.5 [b3mpy][BF<sub>4</sub>] mole fraction, Figure 3. Peak deconvolution in this region leads to the appearance of two peaks, peaks VIb and VII (Table S1, Supporting Information), whose amplitudes and positions are reported in Figure 5 (VIb and VII). Peak VIb blueshifts and decreases its amplitude in an almost linear way with increasing [b3mpy]BF<sub>4</sub> concentration, Figure 5 (VIb), and thus, most of it may be attributed to antisymmetric stretching modes of CH<sub>3</sub> groups bonded to pyridinium rings interacting with [N(CN)<sub>2</sub>] anions. Another remarkable peak appears in the 3050–3075 cm<sup>-1</sup> range (peak VII, Figure 5), which blueshifts and decreases its amplitude with increasing [b3mpy][BF<sub>4</sub>] concentration. Nevertheless, the changes of peak VII are clearly nonlinear, leading to two well-defined regions separated by [b3mpy][BF<sub>4</sub>] concentration around 0.44 [b3mpy][BF<sub>4</sub>] mole fraction (~2.5 mol dm<sup>-3</sup>). For the first region of peak VII (Figure 5), peak amplitude decreases and blueshifts remarkably (~20 cm<sup>-1</sup>) with increasing [b3mpy][BF<sub>4</sub>] concentration, whereas for the second region, amplitude and peak position remain almost constant, and thus, remarkable structural changes may be inferred. We may assign peak VII to symmetric and antisymmetric stretchings of the CH<sub>3</sub> group bonded to the pyridinium ring, but its evolution with mixture composition shows that for [b3mpy][BF<sub>4</sub>] concentrations up to around 2.5 mol dm<sup>-3</sup>, cation–anion interactions are dominated by the presence of [N(CN)<sub>2</sub>] anion, and thus, peak amplitude

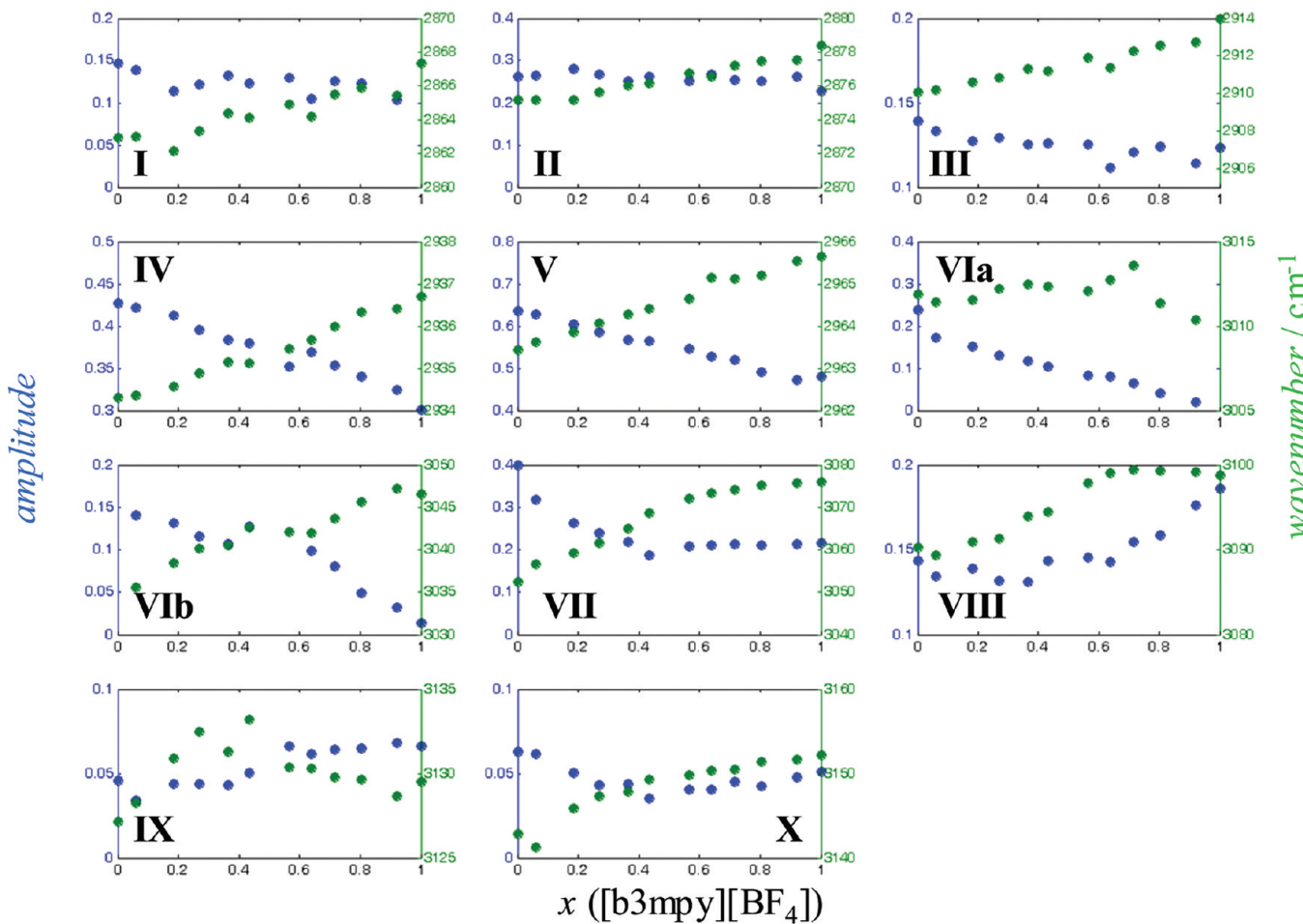


**Figure 5.** Variation of (full circles in green) peak center and (blue) peak amplitude at peak center for the deconvoluted peaks in the 2800–3200  $\text{cm}^{-1}$  range for  $x$  [b3mpy][BF<sub>4</sub>] + (1 -  $x$ ) [b3mpy][N(CN)<sub>2</sub>]. Data obtained from Gaussian–Lorentzian deconvolution of experimental spectra reported in Figure 3.

decreases with increasing [BF<sub>4</sub>] concentration. For [b3mpy][BF<sub>4</sub>] concentrations larger than around 2.5 mol dm<sup>-3</sup>, cation–anion interactions are dominated by the presence of [BF<sub>4</sub>] anion. For the region with [b3mpy][BF<sub>4</sub>] concentration larger than 2.5 mol dm<sup>-3</sup>, the peak properties do not change remarkably with increasing concentration. These results are confirmed by the behavior of the peaks rising from stretching vibrations of CH in the pyridinium ring (peaks VIII to X, Figure 5). Therefore, we may infer that once a critical concentration of [BF<sub>4</sub>] anions is reached ( $\sim$ 2.5 mol dm<sup>-3</sup>), the fluid structuring does not change remarkably, and thus, we may obtain a [b3mpy][BF<sub>4</sub>]<sub>x</sub>[N(CN)<sub>2</sub>]<sub>1-x</sub> mixed ionic liquid with properties close to that in pure [b3mpy][BF<sub>4</sub>] but with lower [BF<sub>4</sub>] concentrations, which is of interest for practical purposes.

The vibrational spectra of pure [o3mpy][BF<sub>4</sub>] is reported in Figure 2c and for [b3mpy]<sub>x</sub>[o3mpy]<sub>1-x</sub>[BF<sub>4</sub>] mixed ionic liquids in Figure 3b. Results of spectra deconvolution are reported in Table S2 (Supporting Information) and the changes of peak amplitude and peak center positions as a function of composition are reported in Figure 6. The spectra deconvolution for pure [o3mpy][BF<sub>4</sub>] led to five peaks in the 2800 to 3000  $\text{cm}^{-1}$  range: 2857, 2873, 2902, 2928, and 2958  $\text{cm}^{-1}$  (peaks I to V), which are assigned to symmetric stretching of CH<sub>2</sub>, symmetric stretching of CH<sub>3</sub>, antisymmetric stretching of CH<sub>2</sub>, Fermi resonance mode of CH<sub>3</sub>, and antisymmetric

stretching of CH<sub>3</sub>, respectively. This peak deconvolution is in agreement with those peaks reported in the literature for 1-octyl-3-methylimidazolium chloride (2858, 2871, 2903, 2929, and 2956  $\text{cm}^{-1}$ ) and are also in certain agreement with values reported in previous paragraphs for [b3mpy][BF<sub>4</sub>], and thus, the peak positions corresponding to alkylic chain vibrations are not remarkably affected neither by the moiety to which they are bonded nor by the type of anion. Spectra deconvolution in the 3000–3200  $\text{cm}^{-1}$  range led to five peaks at 3044, 3075, 3097, 3127, and 3152  $\text{cm}^{-1}$  (peaks VI to X, Table S2, Supporting Information), which correspond to symmetric and antisymmetric stretching of the CH<sub>3</sub> group bonded to the pyridinium ring and to stretching vibrations of CH groups in the pyridinium ring, respectively. Peaks VI to X appear in [o3mpy][BF<sub>4</sub>] at almost the same positions, and their amplitudes are almost the same as those corresponding to [b3mpy][BF<sub>4</sub>] (Table S2, Supporting Information), and thus, the length of the alkylic chain does not change remarkably the vibrational properties of pyridinium rings.

Results reported in Figure 3b for the spectra evolution on going from pure [o3mpy][BF<sub>4</sub>] to pure [b3mpy][BF<sub>4</sub>] show that the main changes happen in the 2800–3000  $\text{cm}^{-1}$  range (peaks I to V), whereas no relevant changes are reported for the 3000–3200  $\text{cm}^{-1}$  range. The variation of the amplitude and center position of the peaks obtained from spectra deconvolution are reported in Figure 6 for

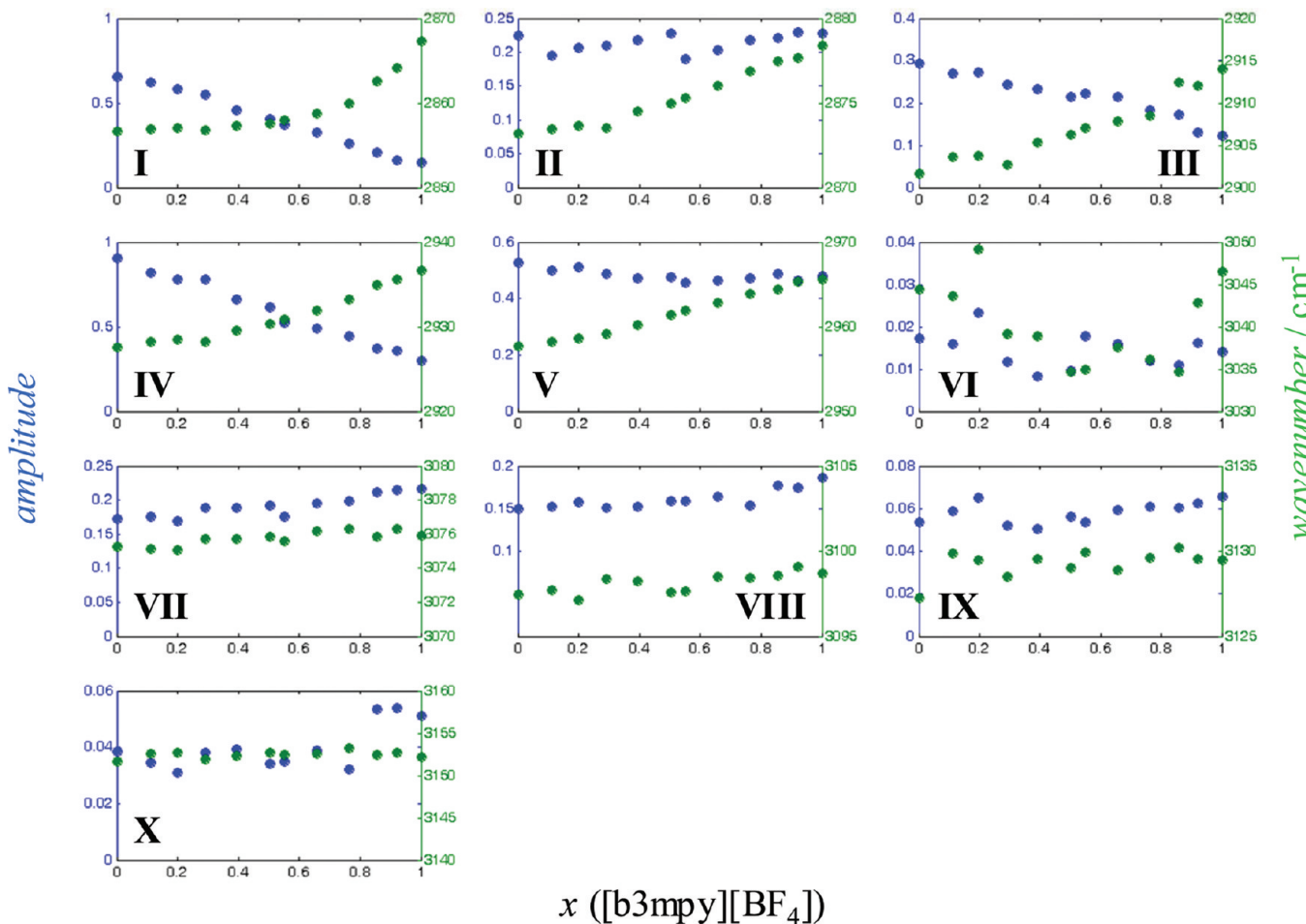


**Figure 6.** Variation of (full circles in green) peak center and (blue) peak amplitude at peak center for the deconvoluted peaks in the 2800–3200  $\text{cm}^{-1}$  range for  $x [\text{b3mpy}][\text{BF}_4] + (1 - x) [\text{o3mpy}][\text{BF}_4]$ . Data obtained from Gaussian–Lorentzian deconvolution of experimental spectra reported in Figure 3.

$[\text{b3mpy}]_x[\text{o3mpy}]_{1-x}[\text{BF}_4]$  with increasing  $[\text{b3mpy}]$  cation concentration, showing that peaks I to V suffer certain changes on going from  $[\text{o3mpy}]$  to  $[\text{b3mpy}]$  cations, especially for the amplitude and in a minor degree for the peak positions. Alkylic  $\text{CH}_2$  symmetric stretching (peak I) blueshifts ( $\sim 10 \text{ cm}^{-1}$ ) on going from  $[\text{o3mpy}][\text{BF}_4]$  to  $[\text{b3mpy}][\text{BF}_4]$ , with the amplitude decreasing in a linear way, Figure 6 (I). Moreover, the blue shifting of peak I is clearly nonlinear, peak position remains almost constant up to 0.6  $[\text{b3mpy}][\text{BF}_4]$  mole fraction ( $2.65 \text{ mol dm}^{-3}$ ), and then it increases with increasing  $[\text{b3mpy}]$  concentration. The second peak (peak II), attributed to symmetric stretching of alkylic  $\text{CH}_3$ , blueshifts ( $\sim 5 \text{ cm}^{-1}$ ) in a linear way, and its amplitude remains almost constant with increasing  $[\text{b3mpy}]$  concentration. Peaks III and V vary in an almost linear way with increasing  $[\text{b3mpy}]$ , and for peak IV, amplitude decreases linearly, and blueshifting ( $\sim 10 \text{ cm}^{-1}$ ) shows a nonlinear behavior with changes from 0.6  $[\text{b3mpy}][\text{BF}_4]$  mole fraction, as with peak I. Therefore, vibrational properties of alkylic chains bonded to pyridinium moieties do not change remarkably with the length of the alkylic chain, only  $\text{CH}_2$  symmetric stretching and Fermi resonance mode show subtle changes from 0.6  $[\text{b3mpy}][\text{BF}_4]$  mole fraction. This behavior points to the existence of apolar domains in which alkylic chains are involved, the average sizes of the chains involved in these domains depend linearly of  $[\text{b3mpy}]_x[\text{o3mpy}]_{1-x}[\text{BF}_4]$  composition, and thus, properties

change in a linear way on going from apolar domains with large chains ( $[\text{o3mpy}]$  dominated regions) to shorter chains ( $[\text{b3mpy}]$  dominated regions). This is confirmed by the behavior of peaks VI to X reported in Figure 6 in which properties remain almost constant in the full composition range.

**3.2. Molecular Dynamics Simulations.** Molecular dynamics simulations were carried for the two binary systems studied in this work,  $[\text{b3mpy}][\text{BF}_4]_x[\text{N}(\text{CN})_2]_{1-x}$  and  $[\text{b3mpy}]_x[\text{o3mpy}]_{1-x}[\text{BF}_4]$ , in the full composition range at isothermal and isobaric conditions (298 K/0.1 MPa). Relevant radial distribution functions, RDFs, are reported in Figure 7 and the corresponding running integrals,  $N$ , in Figures 8 (for the first and second solvation shells) and S1 (Supporting Information, for any distance), for the  $[\text{b3mpy}][\text{BF}_4]_x[\text{N}(\text{CN})_2]_{1-x}$  binary system. Anion–anion interactions are analyzed through the RDFs for the B–B and NC1–NC1 (where NC1 stands for the central nitrogen atom in  $\text{N}(\text{CN})_2^-$  ion) pairs and for the  $\text{BF}_4^-$  and  $\text{N}(\text{CN})_2^-$  anions, respectively, Figure 7a,b. RDFs for anion–anion interactions remain almost constant in the whole composition range, Figure 7a,b, and the corresponding  $N$  values, Figure 8, varies in a linear way with increasing  $\text{BF}_4^-$  concentration, both for the first and second solvation shells (medium and large interaction ranges), which correspond to a simple dilution effect of the corresponding anions with varying concentration, and thus, no remarkable

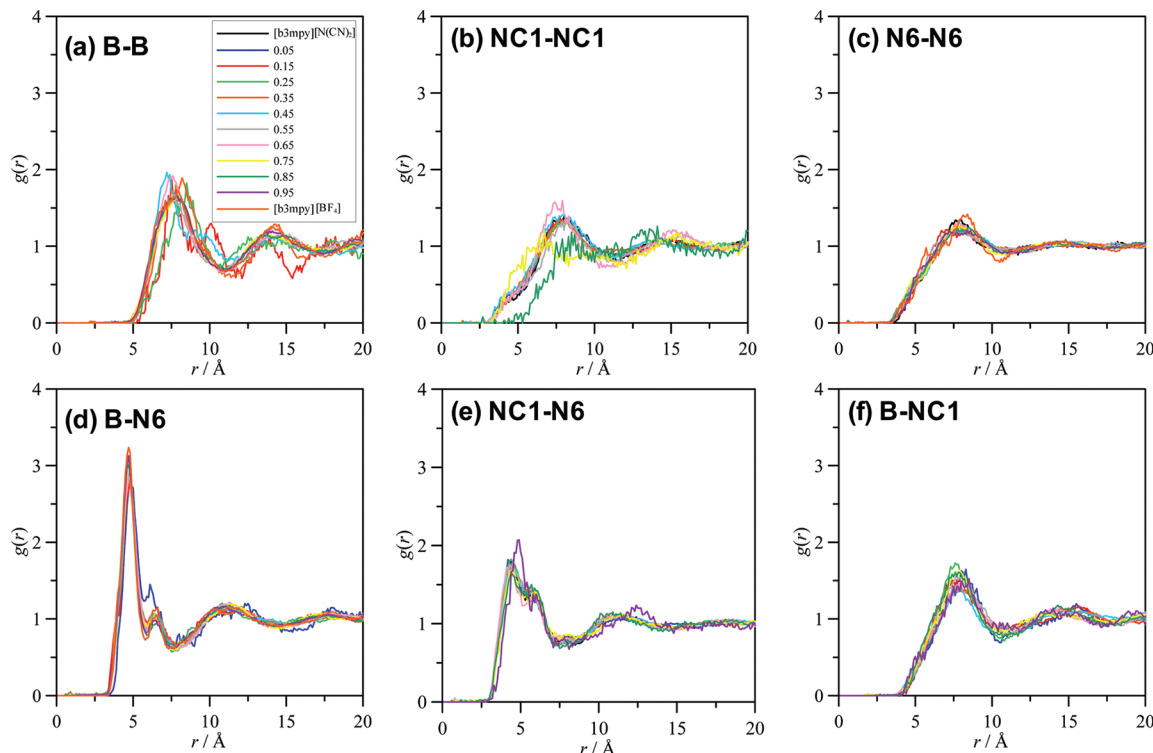


**Figure 7.** Radial distribution functions,  $g(r)$ , for  $x$  [b3mpy][BF<sub>4</sub>] +  $(1 - x)$  [b3mpy][N(CN)<sub>2</sub>] binary mixtures obtained from molecular dynamics simulations at 298 K/0.1 MPa. Lines show results for different values of mole fraction,  $x$ . Atom code: B, boron in BF<sub>4</sub><sup>-</sup> anion; NC1, central nitrogen in [N(CN)<sub>2</sub>] anion; and N6, pyridinium ring nitrogen [b3mpy]<sup>+</sup> cation.

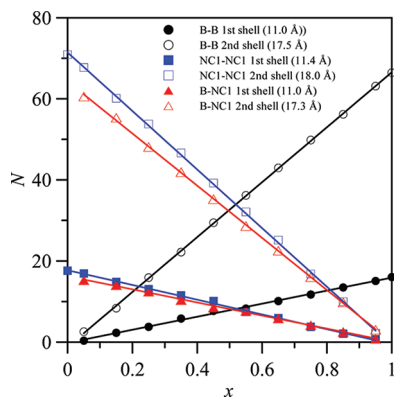


**Figure 8.** Values of running integrals,  $N$ , in the first and second solvation shells for the reported pairs for  $x$  [b3mpy][BF<sub>4</sub>] +  $(1 - x)$  [b3mpy][N(CN)<sub>2</sub>] binary mixtures obtained from molecular dynamics simulations at 298 K/0.1 MPa. Values in angstroms reported within the figure show the position of the first and second minima in radial distribution functions (Figure 7), used to obtain the  $N$  values reported in this figure. Atom code same as that in Figure 7.

structural changes are inferred. Analogous results are obtained for the cation–cation interactions, Figure 7c. Anion–cation interactions show analogous features; Figure 7d,e shows RDFs for anion–cation interactions, considering the anion as the corresponding moiety around which cation distribution is analyzed. For BF<sub>4</sub><sup>-</sup>–[b3mpy]<sup>+</sup> pairs, stronger and narrower RDFs peaks than those corresponding to N(CN)<sub>2</sub><sup>-</sup>–[b3mpy]<sup>+</sup> pairs, are obtained, which point to stronger interaction between the cation and the BF<sub>4</sub><sup>-</sup> anion. Nevertheless, neither the shape nor the intensity of the RDFs for the anion–cation pairs change remarkably with mixture composition, and the corresponding

running integrals remains almost constant in the whole composition range, Figures 8 and S1 (Supporting Information). Therefore, the way in which anions and cations interact do not change with dilution, and both anions interact in the same way with the cation in highly diluted solutions (in which the other anion prevails) and in highly concentrated solutions (in which they prevail), and thus, the anion–cation interaction is not affected by the presence of the other type of anion, at least for the anions considered in this work. The results point to a simple replacement of anions with varying anion concentration around the [b3mpy]<sup>+</sup> cation. The way in which [BF<sub>4</sub>]<sup>-</sup> and [N(CN)<sub>2</sub>]<sup>-</sup> anions interact may be analyzed through the RDFs reported in Figure 7f, which show analogous distribution for all the studied compositions; both anions are placed around the cation and interact in a similar way along the whole composition range with a simple variation rising from anion dilution, Figures 8 and S1 (Supporting Information).

The intermolecular (interionic) interaction energy,  $E_{\text{inter}}$ , for the [b3mpy][BF<sub>4</sub>]<sub>x</sub>[N(CN)<sub>2</sub>]<sub>1-x</sub> system is reported in Figure 9. We reported in a previous work that [b3mpy][BF<sub>4</sub>] and [b3mpy][N(CN)<sub>2</sub>] pure ionic liquids have similar interaction energies, in spite of the large differences between their viscosities.<sup>17</sup> Results reported in Figure 9 show that  $E_{\text{inter}}$  remains almost constant in the whole composition range, and although a minimum appears, it is only a 0.6% of the  $E_{\text{inter}}$  value, which is an almost negligible change with varying mixture concentration.

The behavior of density,  $\rho$ , and excess molar volume,  $V^E$ , is reported in Figure 10. Slight deviations from ideality are obtained, leading to negative excess molar volumes reaching a minimum at equimolar concentrations. Stoppa et al.<sup>16</sup> reported positive excess molar volume for the binary system [1-ethyl-3-methylimidazolium][BF<sub>4</sub>]<sub>x</sub>[N(CN)<sub>2</sub>]<sub>1-x</sub>, which is in contrast

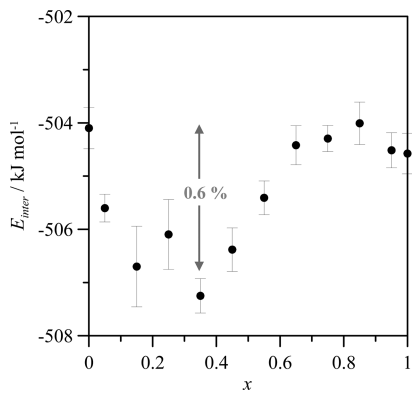


**Figure 9.** Intermolecular energy,  $E_{\text{inter}}$ , for  $x$   $[\text{b3mpy}][\text{BF}_4]$  +  $(1 - x)$   $[\text{b3mpy}][\text{N}(\text{CN})_2]$  binary mixtures obtained from molecular dynamics simulations at 298 K/0.1 MPa. The value in the arrow shows the percentage variation on going from pure ionic liquids to the minimum.

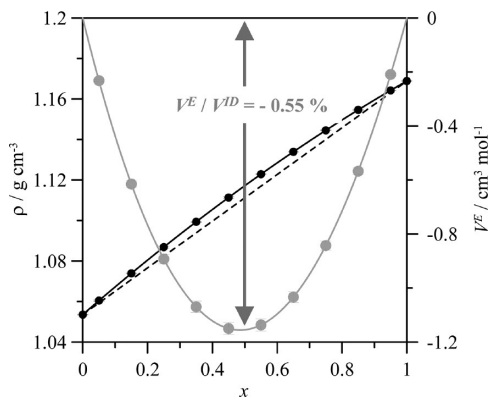


**Figure 10.** Density,  $\rho$ , and excess molar volume,  $V^E$ , for  $x$   $[\text{b3mpy}][\text{BF}_4]$  +  $(1 - x)$   $[\text{b3mpy}][\text{N}(\text{CN})_2]$  binary mixtures obtained from molecular dynamics simulations at 298 K/0.1 MPa. Continuous lines show polynomial fitting for guiding purposes, and the dashed line shows ideal behavior for density.

with the predicted negative values reported in this work for  $[\text{b3mpy}]_{x}[\text{BF}_4]_{1-x}[\text{N}(\text{CN})_2]_{1-x}$ . Likewise,  $V^E/V^{\text{ideal}}$  for  $[\text{1-ethyl-3-methylimidazolium}]_{x}[\text{BF}_4]_{1-x}[\text{N}(\text{CN})_2]_{1-x}$  is lower than 0.1% in the whole composition range, whereas for  $[\text{b3mpy}]_{x}[\text{BF}_4]_{1-x}[\text{N}(\text{CN})_2]_{1-x}$  it is lower than 0.55%. Therefore, although both  $[\text{1-ethyl-3-methylimidazolium}]_{x}[\text{BF}_4]_{1-x}[\text{N}(\text{CN})_2]_{1-x}$  and  $[\text{b3mpy}]_{x}[\text{BF}_4]_{1-x}[\text{N}(\text{CN})_2]_{1-x}$  systems show slight deviations from ideality, the cation has a certain effect on mixture properties, pyridinium-based cations lead to structural changes in comparison with imidazolium-based ones. The presence of a pyridinium cation, with a six-membered ring, in comparison with a five-membered imidazolium ring, may lead to larger void spaces in which involved anions may fit more properly leading to negative  $V^E$  values. Moreover, the presence of two nitrogen atoms in the imidazolium ring together with the well-known hydrogen bonding donor ability of the hydrogen atom placed in the C2 position (between both nitrogens) may lead to changes in the involved intermolecular forces with varying mixture composition. The  $[\text{BF}_4]^-$  anion should lead to stronger hydrogen bonding than  $[\text{N}(\text{CN})_2]^-$ , and thus, the presence of the hydrogen in the imidazolium C2 position should lead to a stronger tendency to develop hydrogen bonding with the  $[\text{BF}_4]^-$  anion in comparison with the  $[\text{N}(\text{CN})_2]^-$  one. For the pyridinium-based cation, the absence of strong hydrogen bonding donor positions should lead to lower preferential

interaction with both anions, which is confirmed by the intermolecular energy reported in Figure 9, and thus,  $V^E$  should be controlled basically by steric effects. This is confirmed by the distribution of cavity sizes for the studied pure ionic liquid reported in Figure 11, which was calculated according to the method proposed by Margulis (measuring the smallest distance

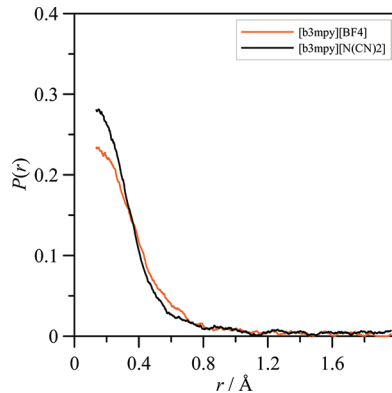


**Figure 11.** Distribution of cavity sizes in  $[\text{b3mpy}][\text{N}(\text{CN})_2]$  and  $[\text{b3mpy}][\text{BF}_4]$  pure ionic liquids obtained from molecular dynamics simulations at 298 K/0.1 MPa.

of random points to all atoms in the liquid).<sup>29</sup> Results reported in Figure 11 shows larger cavities for pure  $[\text{b3mpy}][\text{N}(\text{CN})_2]$  than for  $[\text{b3mpy}][\text{BF}_4]$ , which is in agreement with the stronger anion–cation interactions for  $[\text{b3mpy}][\text{BF}_4]$ . Nevertheless, these differences appear only for short distances, whereas for larger distances, cavity distributions are almost equivalent for both fluids. Therefore, the negative  $V^E$  values reported in Figure 10 could be justified considering the results reported in Figure 11 through the trend to more compact packings on going from pure  $[\text{b3mpy}][\text{N}(\text{CN})_2]$  to  $[\text{b3mpy}][\text{BF}_4]$ , and considering a rearrangement of cavity distribution with increasing  $[\text{b3mpy}][\text{BF}_4]$  mole fraction.

The analysis of dynamic properties for the studied mixed fluids was done through the predicted self-diffusion coefficients,  $D$ , obtained from molecular dynamics simulations using the Einstein's relationship, eq 4

$$D = \frac{1}{6} \lim_{t \rightarrow \infty} \frac{d}{dt} \langle (\Delta r(t))^2 \rangle \quad (4)$$

where the quantity in brackets is mean square displacement, msd. Long simulations are required to obtain reliable  $D$  values from msd results due to the sluggish behavior of ionic liquids,<sup>30</sup> especially for the mixtures rich in  $[\text{b3mpy}][\text{BF}_4]$ , where viscosity is almost 8-fold that of  $[\text{b3mpy}][\text{N}(\text{CN})_2]$ . The  $\beta$  parameter, defined according to eq 5,<sup>31</sup> is very useful to analyze if the diffusive regime has been reached in the evolution of msd with time, and thus, to infer if calculated  $D$  values are accurate.

$$\beta(t) = \frac{d \log_{10} \langle (\Delta r(t))^2 \rangle}{d \log_{10} t} \quad (5)$$

All the simulations carried out in this work led to  $\beta$  values in the range 0.7 to 0.8, and thus, a subdiffusive regime is analyzed. Nevertheless, as the objective of the work is not to infer  $D$  values but to analyze the changes with mixture composition, we may consider the predicted  $D$  values as useful to analyze possible structural and dynamic changes upon mixing. Anion and cation  $D$  values are reported in Figure 12.  $D$  values for the

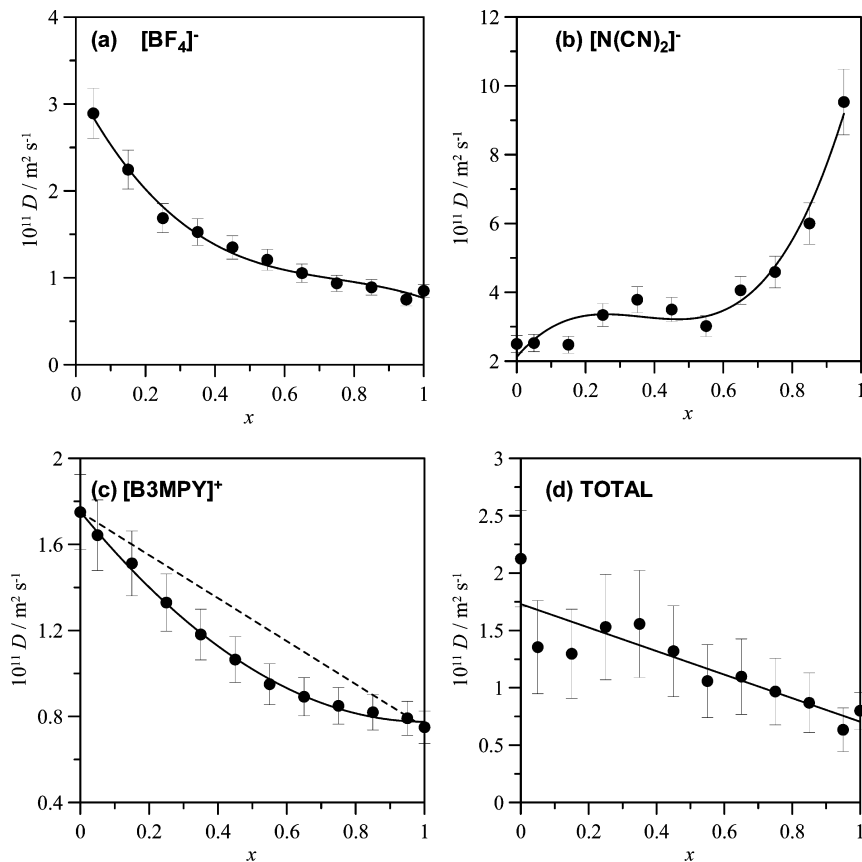


**Figure 12.** Self-diffusion coefficient,  $D$ , for the anions, cation, and total fluid, in  $x [\text{b3mpy}][\text{BF}_4] + (1 - x) [\text{b3mpy}][\text{N}(\text{CN})_2]$  binary mixtures, obtained from molecular dynamics simulations at 298 K/0.1 MPa. Total  $D$  values are obtained from composition averaged values of the anions and cation. In panels a–c, continuous lines show polynomial fits for guiding purposes; in panel c, a dashed line shows linear behavior, and in panel d, a continuous line shows linear fit for guiding purposes.

$[\text{BF}_4]^-$  anion, Figure 12a, decrease with increasing  $[\text{b3mpy}][\text{BF}_4]$  concentration up to 0.5 mol fraction, and then it remains almost constant up to the pure  $[\text{b3mpy}][\text{BF}_4]$  ionic liquid. A similar behavior is obtained for  $\text{N}(\text{CN})_2^-$  anion, Figure 12b: almost constant for  $[\text{b3mpy}][\text{N}(\text{CN})_2]$  rich mixtures and then increasing from equimolar concentrations with increasing  $[\text{b3mpy}][\text{BF}_4]$  mole fraction. Therefore, anion mobility is large for diluted mixtures, especially for  $[\text{N}(\text{CN})_2^-]$  anion, whereas dynamic behavior seems to be clearly separated by equimolar concentrations: a zone rich in  $[\text{N}(\text{CN})_2^-]$  and another one dominated by  $[\text{BF}_4]^-$  anions. Cation  $D$  values, Figure 12, decrease in a nonlinear way from the larger values of  $[\text{b3mpy}][\text{N}(\text{CN})_2]$  to the lower values of  $[\text{b3mpy}][\text{BF}_4]$ . Values for  $D/D_{\text{linear}}$  lead to a minimum for equimolar composition, and deviations for linearity are lower than 20% in the whole composition range. Therefore, changes on the diffusion behavior rises following a nonlinear behavior, which could be justified considering the different behavior of RDFs for  $[\text{b3mpy}][\text{BF}_4]$  and  $[\text{b3mpy}][\text{N}(\text{CN})_2]$  pairs reported in Figure 7d,e, which point to stronger  $[\text{b3mpy}][\text{BF}_4]$  interactions. Nevertheless, the self-diffusion coefficient for the mixture (calculated from the composition averaged  $D$  values for all the involved ions) evolves in an almost linear way, Figure 12d, and thus, dynamic properties of the mixed ionic liquids change with a linear dilution type behavior, as the remaining properties studied for these mixed fluids. Therefore,  $[\text{b3mpy}][\text{BF}_4][\text{N}(\text{CN})_2]_{1-x}$  systems change in an almost linear way for most of the studied properties, and thus point to a simple

dilution effect to justify the changes on the behavior of the studied systems.

Molecular dynamics results for the  $[\text{b3mpy}]_x[\text{o3mpy}]_{1-x}[\text{BF}_4]$  mixed ionic liquid may lead to information about the structural changes rising from the increasing presence of a large alkylic chain in the pyridinium cation, the possible effect of increasing apolar domains with increasing  $[\text{o3mpy}]^+$  concentration, and the effect of these possible apolar domains and larger alkylic chains on the anion–cation interactions. Relevant RDFs are reported in Figure 13, the reported results do not show relevant changes with mixture composition. Anion–anion RDFs remain constant in the full composition range, Figure 13a; likewise, cation–cation RDFs, Figure 13b,c, are almost equal both for imidazolium cations with butyl and octyl side chains. Moreover,  $\text{BF}_4^-$  anion interacts in an analogous way both with  $[\text{b3mpy}]^+$  and  $[\text{o3mpy}]^+$  cation, Figure 13d,e. Therefore, the increasing length of the alkylic side chain does not lead to remarkable structural changes in the mixed fluids, and the way in which ions interact remains almost unchanged in the full composition range. The possible appearance of apolar domains formed by alkylic chains are analyzed in Figure 13f, in which RDFs for the terminal carbons in butyl and octyl chains is reported; results show a certain degree of ordering inferred from the RDFs peak appearing at around 4.7–5.0 Å. Intermolecular (interionic) interaction energy is reported in Figure 14.  $E_{\text{inter}}$  is larger (in absolute value) for pure  $[\text{o3mpy}][\text{BF}_4]$  ( $-509.2 \text{ kJ mol}^{-1}$ ) than for pure  $[\text{b3mpy}][\text{BF}_4]$  ( $-504.6 \text{ kJ mol}^{-1}$ ), although the difference is

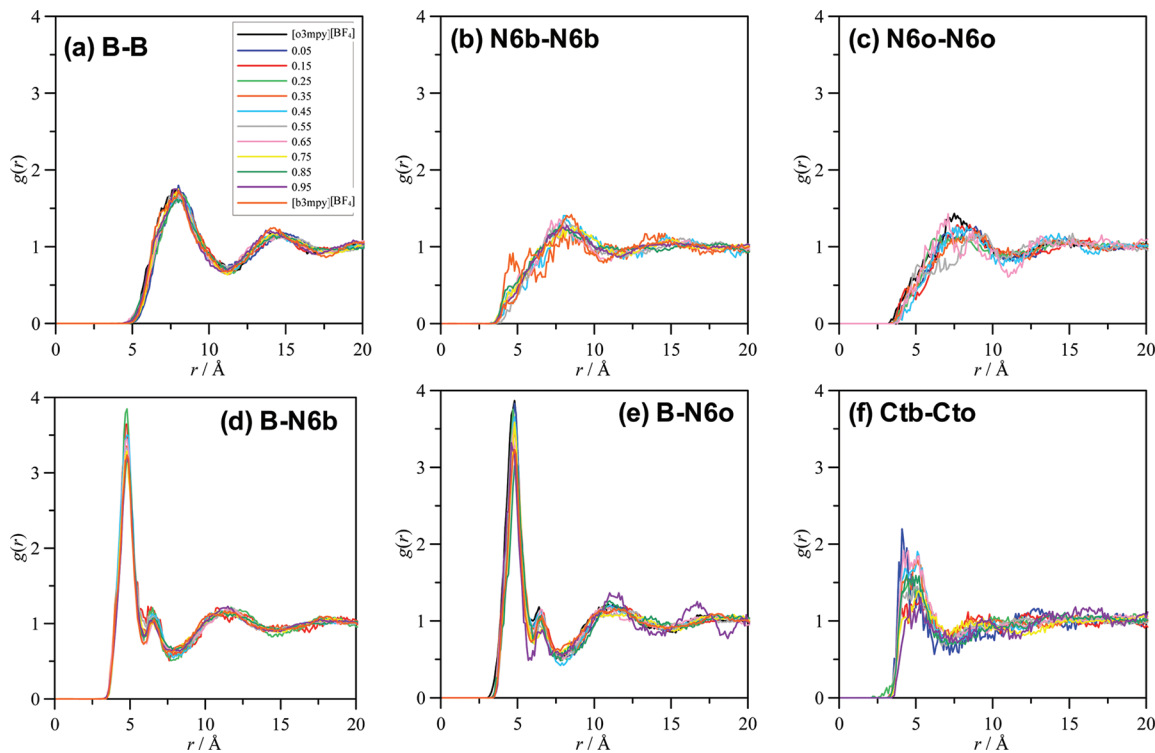


**Figure 13.** Radial distribution functions,  $g(r)$ , for  $x$  [b3mpy][BF<sub>4</sub>] + (1 -  $x$ ) [o3mpy][BF<sub>4</sub>] binary mixtures obtained from molecular dynamics simulations at 298 K/0.1 MPa. Lines show results for different values of mole fraction,  $x$ . Atom code: B, boron in BF<sub>4</sub><sup>-</sup> anion; N6b, pyridinium ring nitrogen in [b3mpy] cation; N6o, pyridinium ring nitrogen in [o3mpy] cation; Ctb, terminal carbon in butyl chain in [b3mpy] cation; and Cto, terminal carbon in octyl chain in [o3mpy] cation.

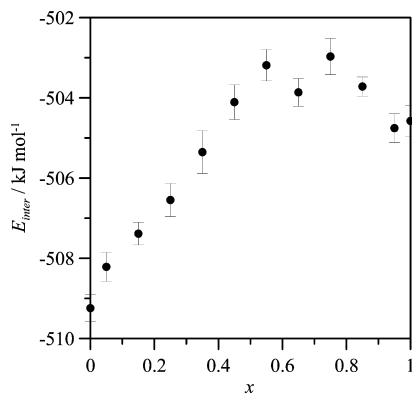


**Figure 14.** Intermolecular energy,  $E_{\text{inter}}$ , for  $x$  [b3mpy][BF<sub>4</sub>] + (1 -  $x$ ) [o3mpy][BF<sub>4</sub>] binary mixtures obtained from molecular dynamics simulations at 298 K/0.1 MPa.

just a 0.9%. With increasing [b3mpy][BF<sub>4</sub>] mole fraction,  $E_{\text{inter}}$  increases in a linear way up to equimolar composition from which it remains almost constant. Therefore, from the energetic and structural viewpoints [b3mpy]<sub>x</sub>[o3mpy]<sub>1-x</sub>[BF<sub>4</sub>] behaves as an almost ideal system. Nevertheless, pure [o3mpy][BF<sub>4</sub>] is less dense than pure [b3mpy][BF<sub>4</sub>], and thus, with increasing [b3mpy][BF<sub>4</sub>] concentration, more efficiently packed fluids should rise. We have analyzed this effect in Figure 15, in which predicted density and excess molar volume are reported. Density behaves in a nonlinear way, which leads to positive excess molar volume. This expansive behavior may be justified considering the steric hindrance rising from the presence of octyl chains. Nevertheless, the  $V^E/V^{\text{ideal}}$  is just a 0.36%. Canongia et al.<sup>12</sup> reported positive excess molar volume for

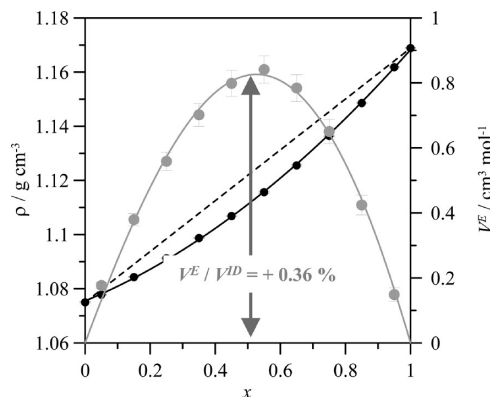


**Figure 15.** Density,  $\rho$ , and excess molar volume,  $V^E$ , for  $x$  [b3mpy][BF<sub>4</sub>] + (1 -  $x$ ) [o3mpy][BF<sub>4</sub>] binary mixtures obtained from molecular dynamics simulations at 298 K/0.1 MPa. Continuous lines show polynomial fitting for guiding purposes, and a dashed line shows ideal behavior for density.

mixtures of [C<sub>2</sub>mim][Tf<sub>2</sub>N] + [C<sub>10</sub>mim][Tf<sub>2</sub>N], with a maximum at equimolar composition of 0.27 cm<sup>3</sup> mol<sup>-1</sup>, which is lower than the 0.84 cm<sup>3</sup> mol<sup>-1</sup> obtained in this work for [b3mpy]<sub>x</sub>[o3mpy]<sub>1-x</sub>[BF<sub>4</sub>]. Therefore, mixed ionic liquids based on alkylpyridinium cations lead to larger expansions than those based on alkylimidazolium cations. The evolution of possible apolar domains with mixture composition is analyzed in Figure 16. The snapshots reported for pure [o3mpy][BF<sub>4</sub>], Figure 16a, and pure [b3mpy][BF<sub>4</sub>], Figure 16e, show the larger extension of apolar regions (green zones) in pure [o3mpy][BF<sub>4</sub>], as we may have expected from the presence of larger alkyl side chains, whereas in pure

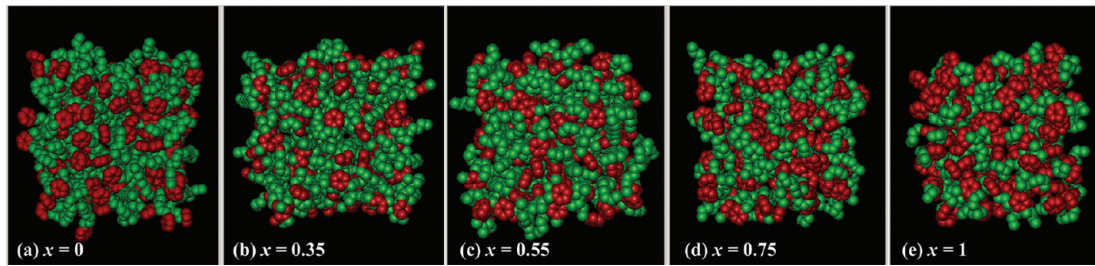


**Figure 16.** Snapshots of simulation boxes of  $x$  [b3mpy][BF<sub>4</sub>] + (1 -  $x$ ) [o3mpy][BF<sub>4</sub>] binary mixtures obtained from molecular dynamics simulations at 298 K/0.1 MPa. Color code: red, imidazolium rings, and green, alkyl side chains in [b3mpy]<sup>+</sup> and [o3mpy]<sup>+</sup> cations. [BF<sub>4</sub>]<sup>-</sup> anions are omitted for the sake of visibility.

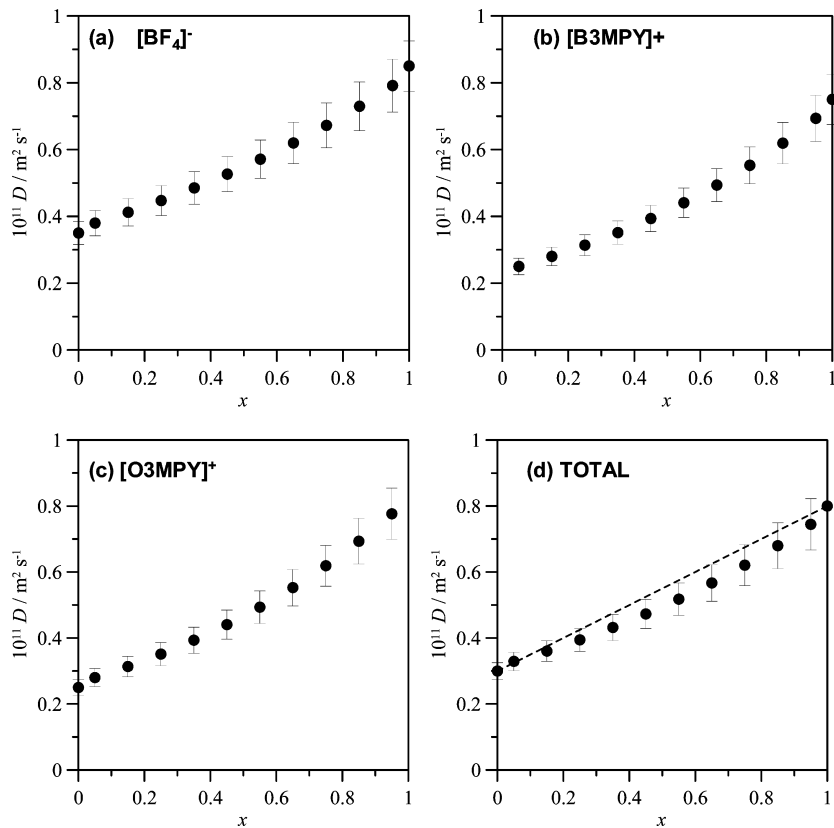


**Figure 17.** Self-diffusion coefficient,  $D$ , for the anions, cation, and total fluid, in  $x$  [b3mpy][BF<sub>4</sub>] + (1 -  $x$ ) [o3mpy][BF<sub>4</sub>] binary mixtures, obtained from molecular dynamics simulations at 298 K/0.1 MPa. Total  $D$  values are obtained from composition averaged values of the anions and cation. In panel d, the dashed line shows linear behavior.

[b3mpy][BF<sub>4</sub>], apolar and polar (red areas) seem to be more interpenetrated. With increasing [b3mpy][BF<sub>4</sub>] mole fraction, Figure 16b-d, the extension of apolar domains seems to decrease, and increasing mixing of apolar and polar domains rise on going toward pure [b3mpy][BF<sub>4</sub>]. Self-diffusion coefficients as a function of mixture composition are reported in Figure 17. It should be remarked that [o3mpy][BF<sub>4</sub>] is 2.6 times more viscous than [b3mpy][BF<sub>4</sub>] (at 293.15 K),<sup>17</sup> and thus, increases in [b3mpy][BF<sub>4</sub>] mole fraction should lead to remarkable increases in self-diffusion coefficients. Anion and cation  $D$  values reported in Figure 17 evolve in an almost linear way with increasing [b3mpy][BF<sub>4</sub>] mole fraction, which is in agreement with the properties reported in previous sections. The self-diffusion coefficient for the mixture, Figure 17d, evolves in an almost linear way, with low deviations from the linear behavior (lower than 10%), which should lead to positive deviations from the linear behavior for mixture viscosity.

#### 4. CONCLUSIONS

We reported in this study an ATR-FTIR study combined with molecular dynamics simulations of [b3mpy][BF<sub>4</sub>]<sub>x</sub>[N(CN)<sub>2</sub>]<sub>1-x</sub> and [b3mpy]<sub>x</sub>[o3mpy]<sub>1-x</sub>[BF<sub>4</sub>] mixed ionic liquids. The study of b3mpy][BF<sub>4</sub>]<sub>x</sub>[N(CN)<sub>2</sub>]<sub>1-x</sub> allows analysis of the effect of changing anions and, [b3mpy]<sub>x</sub>[o3mpy]<sub>1-x</sub>[BF<sub>4</sub>], the effect of changing cations, through increasing alkyllic side chains, on mixed ionic liquids properties and structure.

ATR-FTIR results on [b3mpy][BF<sub>4</sub>]<sub>x</sub>[N(CN)<sub>2</sub>]<sub>1-x</sub> show two well-defined regions in which properties resemble those of pure ionic liquids, separated by a critical concentration of [BF<sub>4</sub>] anions ( $\sim 2.5$  mol dm<sup>-3</sup>). The fluid structuring does not change remarkably once this critical concentration is reached. Molecular dynamics results confirm the ATR-FTIR results, showing that properties for [b3mpy][BF<sub>4</sub>]<sub>x</sub>[N(CN)<sub>2</sub>]<sub>1-x</sub> systems change in an almost linear way, leading to an almost ideal mixture from the thermodynamic viewpoint, pointing to a

simple dilution effect of the involved anions leading to regions dominated by interactions between  $[b3mpy]^+$  and  $[N(CN)_2]^-$  ions, in which  $BF_4^-$  are dispersed, or reverse for regions dominated by  $[b3mpy]^+$  and  $[BF_4]^-$  ions.

For the  $[b3mpy]_x[03mpy]_{1-x}[BF_4]$  mixed system, ATR-FTIR results point to the existence of apolar domains; the average sizes of the alkylidic side chains involved in these domains evolve linearly with mixture mole fraction, decreasing with increasing  $[b3mpy][BF_4]$  concentration. Molecular dynamics results point to very weak structural changes with increasing  $[b3mpy][BF_4]$  concentration, rising from the decreasing size of apolar domains, which lead to positive excess molar volume, but without important changes in the way in which ions interacts or in the energetic properties of the systems. Therefore, the properties of  $[b3mpy]_x[03mpy]_{1-x}[BF_4]$  mixed systems may be simply explained considering lower apolar domains for  $[b3mpy][BF_4]$  rich systems, which lead to more efficient packings, lower steric hindrance, more dense and less viscous fluids, but without important structural changes.

The results reported in this work show that properties of ionic liquids may be adjusted not only by suitable combinations of anions and cations but also through the development of ionic liquids with several anions and cations at selected composition. The scarcely available studies in the literature recommend the development of systematic experimental-computational studies on mixed ionic liquids to advance in the knowledge of these complex systems.

## ASSOCIATED CONTENT

### Supporting Information

Results of spectra deconvolution for  $[b3mpy][BF_4]_x[N(CN)_2]_{1-x}$  and  $[b3mpy]_x[03mpy]_{1-x}[BF_4]$  mixtures in the full composition range; Running integrals for  $[b3mpy]-[BF_4]_x[N(CN)_2]_{1-x}$  obtained from molecular dynamics simulations. This material is available free of charge via the Internet at <http://pubs.acs.org>.

## AUTHOR INFORMATION

### Corresponding Author

\*E-mail: sapar@ubu.es.

### Notes

The authors declare no competing financial interest.

## ACKNOWLEDGMENTS

We acknowledge the financial support by the Ministerio de Ciencia e Innovación, Spain (Project CTQ2010-15871) and by the NPRP grant (No. NPRP-09-739-2-284) from the Qatar National Research Fund.

## REFERENCES

- (1) Pleckkova, N. V.; Seddon, K. R. *Chem. Soc. Rev.* **2008**, *37*, 123.
- (2) Werner, H. M.; Wassercheid, P. *Annu. Rev. Chem. Biomol. Eng.* **2010**, *1*, 203.
- (3) Torimoto, T.; Tsuda, T.; Okazaki, K.; Kuwabata, S. *Adv. Mater.* **2010**, *22*, 1196.
- (4) Castner, E. W.; Wishart, J. F. *J. Chem. Phys.* **2010**, *132*, 120901.
- (5) Kristen, C. J.; Pieraccini, D.; Stara, A.; Chiappe, C.; Arlt, W. *J. Chem. Thermodyn.* **2005**, *37*, 537.
- (6) Mohanty, S.; Banerjee, T.; Mohanty, K. *Ind. Eng. Chem. Res.* **2010**, *49*, 2916.
- (7) Moniruzzaman, M.; Nakashima, K.; Goto, M. *Biochem. Eng. J.* **2010**, *48*, 295.
- (8) Zhao, H. *Chem. Eng. Commun.* **2006**, *193*, 1660.
- (9) Baker, G. A.; Baker, S. N.; Pandey, S.; Bright, F. V. *Analyst* **2005**, *130*, 800.
- (10) Rooney, D. W.; Jacquemin, J.; Gardas, R. *Top. Curr. Chem.* **2010**, *290*, 185.
- (11) Fletcher, K. A.; Baker, S. N.; Baker, G. A.; Pandey, S. *New. J. Chem.* **2003**, *27*, 1706.
- (12) Canongia, J. N.; Cordeiro, T. C.; Esperanca, J. M. S. S.; Guedes, H. J. R.; Huq, S.; Rebelo, L. P. N.; Seddon, K. R. *J. Phys. Chem. B* **2005**, *109*, 3519.
- (13) Xiao, D.; Rajian, J. R.; Hines, L. G.; Bartsch, R. A.; Quitevis, E. *L. J. Phys. Chem. B* **2008**, *112*, 13316.
- (14) Finotello, A.; Bara, J. E.; Narayan, S.; Camper, D.; Noble, R. D. *J. Phys. Chem. B* **2008**, *112*, 2335.
- (15) Navia, P.; Troncoso, J.; Román, L. *J. Sol. Chem.* **2008**, *37*, 677.
- (16) Stoppa, A.; Buchner, R.; Hefta, G. *J. Mol. Liq.* **2010**, *153*, 46.
- (17) Aparicio, S.; Alcalde, R.; Lafuente, C.; Bandrés, I.; Atilhan, M. *J. Phys. Chem. B* **2011**, *115*, 12499.
- (18) Aparicio, S.; Alcalde, R.; Atilhan, M. *J. Phys. Chem. B* **2010**, *114*, 5795.
- (19) Aparicio, S.; Atilhan, M.; Kraishev, M.; Alcalde, R. *J. Phys. Chem. B* **2011**, *115*, 12473.
- (20) Ponder, J. W. *TINKER: Software Tool for Molecular Design*, 4.2 ed; Washington University School of Medicine: St. Louis, MO, 2004.
- (21) Hoover, W. G. *Phys. Rev. A* **1985**, *31*, 1695.
- (22) Allen, M. P.; Tildesley, D. J. *Computer Simulation of Liquids*; Clarendon Press: Oxford, UK, 1989.
- (23) Essmann, U. L.; Perera, M. L.; Berkowitz, T.; Darden, H.; Lee, H.; Pedersen, L. G. *J. Chem. Phys.* **1995**, *103*, 8577.
- (24) Martínez, J. M.; Martínez, L. *J. Comput. Chem.* **2003**, *24*, 819–825.
- (25) Jeon, Y.; Sung, J.; Kim, D.; Seo, C.; Cheong, H.; Ouchi, Y.; Ozawa, R.; Hamaguchi, H. *J. Phys. Chem. B* **2008**, *112*, 923.
- (26) Hasse, B.; Lehmann, J.; Assenbaum, D.; Wassercheid, P.; Leipertz, A.; Fröba, A. *P. J. Chem. Eng. Data* **2009**, *54*, 2576.
- (27) Jeon, Y.; Sung, J.; Seo, C.; Lim, H.; Cheong, H.; Kang, M.; Moon, B.; Kim, D. *J. Phys. Chem. B* **2008**, *112*, 4735.
- (28) Kovacs, A. *J. Mol. Struct.* **1999**, *482–483*, 397.
- (29) Margulis, C. *J. Mol. Phys.* **2004**, *102*, 829.
- (30) Del-Popolo, M. G.; Voth, G. A. *J. Phys. Chem. B* **2004**, *108*, 1744.
- (31) Hu, Z.; Margulis, C. *Proc. Natl. Acad. Sci. U.S.A.* **2006**, *103*, 831.